Talanta 232 (2021) 122395

Contents lists available at ScienceDirect

Talanta

journal homepage: www.elsevier.com/locate/talanta

A dual-colored persistent luminescence nanosensor for simultaneous and autofluorescence-free determination of aflatoxin B_1 and zearalenone

Yuan-Yuan Jiang [a,b,c], Xu Zhao [a,b,c,d], Li-Jian Chen [a,b,c,d], Cheng Yang [a,b,c], Xue-Bo Yin [e], Xiu-Ping Yan [a,b,c,d,*]

[a] State Key Laboratory of Food Science and Technology, Jiangnan University, Wuxi, 214122, China
[b] International Joint Laboratory on Food Safety, Jiangnan University, Wuxi, 214122, China
[c] Institute of Analytical Food Safety, School of Food Science and Technology, Jiangnan University, Wuxi, 214122, China
[d] Key Laboratory of Synthetic and Biological Colloids, Ministry of Education, Jiangnan University, Wuxi, 214122, China
[e] Research Center for Analytical Science, College of Chemistry, Nankai University, Tianjin, 300071, China

ARTICLE INFO

Keywords:
Persistent luminescence nanoparticles
Nanosensor
Autofluorescence-free
Simultaneous biosensing
Mycotoxins

ABSTRACT

Mycotoxins contamination in agricultural products poses a serious threat to human and animal health, so rapid and sensitive nanosensors for simultaneous determination of multiple mycotoxins in food samples are highly desirable for food safety monitoring. Herein, we report the fabrication of functional dual-colored persistent luminescence nanoparticles (PLNPs) in conjunction with Fe_3O_4 magnetic nanoparticles as a nanosensor for the simultaneous biosensing of aflatoxin B_1 (AFB_1) and zearalenone (ZEN) in food samples. Two types of PLNPs with a single excitation wavelength, $Zn_2GeO_4:Mn^{2+}$ and $Zn_{1.25}Ga_{1.5}Ge_{0.25}O_4:Cr^{3+},Yb^{3+},Er^{3+}$, are employed as the signal units, and aptamers with high affinity and specificity to the corresponding mycotoxins are used as the recognition units. The nanosensor was fabricated by hybridizing the aptamer modified PLNPs with the complementary DNA modified Fe_3O_4. The developed nanosensor offers the integrated merits of autofluorescence-free detection of persistent luminescence, the high specificity of aptamer and the high speed of magnetic separation, allowing highly sensitive and selective detection of AFB_1 and ZEN in food samples with the limits of detection of 0.29 pg mL^{-1} for AFB_1 and 0.22 pg mL^{-1} for ZEN and the recoveries of 93.6%–103.2% for AFB_1 and 94.7%–105.1% for ZEN. This work also provides a novel universal PLNPs-based optical platform for the simultaneous detection of multiple contaminants in complex samples.

1. Introduction

Mycotoxins are a class of toxic secondary metabolites produced by certain fungal species that exhibit potential carcinogenicity, neurotoxicity, teratogens, and hepatoxicity [1–3]. Mycotoxins contamination is a critical issue in food safety as cereals such as corn, wheat, rice and peanuts are often contaminated by mycotoxins during growth and storage [4–6]. Cereals are often contaminated by more than one mycotoxin, leading to additional or synergistic toxic effect on humans and animals [7,8]. Moreover, some mycotoxins are hard to destroy due to their potent thermostability [9]. Therefore, it is necessary to develop highly sensitive and rapid techniques for monitoring the possible contamination of mycotoxins. Compared with just single mycotoxin detection in one analytical run, development of analytical methods for simultaneous detection of multiple mycotoxins is highly imperative and significant.

Currently available methods for simultaneous determination of multiple mycotoxins include fluorescent aptasensor [10–12], high performance liquid chromatography [13], liquid chromatography-tandem mass spectrometry [14,15], immunochromatographic assay [16,17] and electrochemical assay [18,19]. Fluorescent assay is increasingly used because of its simplicity, high sensitivity, and rapid analysis. However, most fluorescent methods require continuous excitation light irradiation to produce fluorescent signals, and thus suffer from potential interferences of autofluorescence from complex sample matrixes produced by constant excitation. Therefore, it is essential to establish a practical method for autofluorescence-free determination of trace mycotoxins in complicated food samples.

Persistent luminescence nanoparticles (PLNPs) exhibit long-lasting luminescence after excitation stops, which allows the detection with

* Corresponding author. State Key Laboratory of Food Science and Technology, Jiangnan University, Wuxi, 214122, China.
E-mail address: xpyan@jiangnan.edu.cn (X.-P. Yan).

https://doi.org/10.1016/j.talanta.2021.122395
Received 21 February 2021; Received in revised form 24 March 2021; Accepted 31 March 2021
Available online 14 April 2021

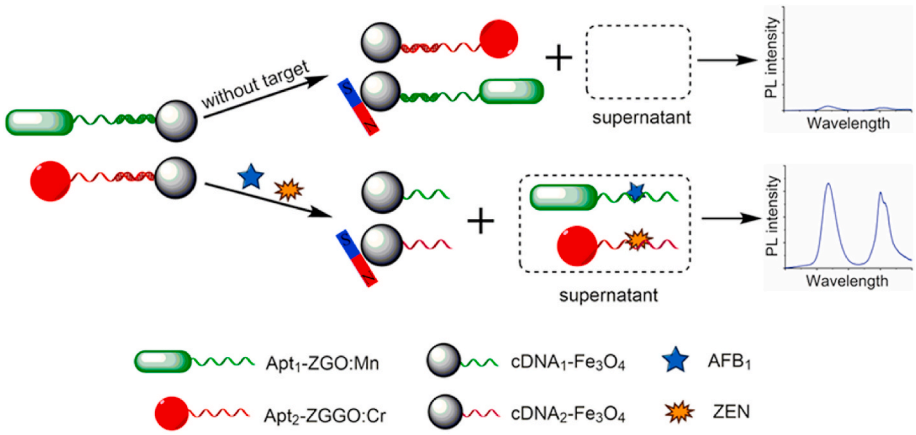

Scheme 1. Schematic for the dual-colored PLNPs based nanosensor for simultaneous detection of ZEN and AFB_1.

no need for in situ excitation, and avoids the interferences from autofluorescence and scattering light in complex matrixes [20–23]. In 2011, our group first reported a PLNPs-based fluorescence resonance energy transfer inhibition assay for the detection of α-fetoprotein [24], which inspired the research on PLNPs-based optical detection. After that, several PLNPs-based optical sensors were reported in succession, including detection of tumor markers [25–28], food-borne hazardous substances [29–32] and reactive species [33,34]. So far, the PLNPs-based optical sensors are still limited. Especially, multiple-colored persistent luminescence nanosensors for the simultaneous detection of two or more mycotoxins have not been reported yet.

Herein, we report a rapid and sensitive multiple-colored persistent luminescence nanosensor for simultaneous determination of two mycotoxins in food samples by integrating functionalized dual-colored persistent luminescence nanoparticles with Fe_3O_4 magnetic nanoparticles (Scheme 1). In this assay, aflatoxin B_1 (AFB_1) and zearalenone (ZEN), two mycotoxins that often naturally co-occur in cereals, are chosen as the targets for their severe damage and toxicity to human health. Two types of PLNPs with a single excitation wavelength, $Zn_2GeO_4:Mn^{2+}$ (ZGO:Mn) and $Zn_{1.25}Ga_{1.5}Ge_{0.25}O_4:Cr^{3+},Yb^{3+},Er^{3+}$ (ZGGO:Cr), are employed as the signal units, and aptamers with high specificity and affinity to the corresponding mycotoxins are used as the recognition units. The aptamer modified PLNPs (Apt-PLNPs) are hybridized with the complementary DNA modified Fe_3O_4 (cDNA-Fe_3O_4) to form two couples of Apt-PLNPs@cDNA-Fe_3O_4 nanocomposites. In the presence of AFB_1 or ZEN, the aptamer can specifically bind to the corresponding mycotoxin and cDNA-Fe_3O_4 will be replaced. The persistent luminescence of the released signal units in supernatant increases with the concentration of the mycotoxins, allowing simultaneous determination of trace ZEN and AFB_1 in food samples without autofluorescence interference.

2. Experimental section

2.1. Reagents and materials

(3-aminopropyl)triethoxysilane (APTES), 4-(2-hydroxyethyl)-1-piperazineethanesulfonic acid (HEPES) and 4-(*N*-maleimidomethyl) cyclohexane-1-carboxylic acid 3-sulfo-*N*-hydroxysuccinimide ester sodium salt (Sulfo-SMCC) came from Aladdin (Shanghai, China). The aptamers with sequences of 5′-SH-GTT GGG CAC GTG TTG TCT CTC TGT GTC TCG TGC CCT TCG CTA GGC CCA CA-3’ (Apt_1, specific for AFB_1) [35], 5′-SH-TCA TCT ATC TAT GGT ACA TTA CTA TCT GTA ATG TGA TAT G-3’ (Apt_2, specific for ZEN) [36], and their corresponding partial complementary DNA with sequences of 5′-SH-GGG CCT AGC GAA GGG C-3’ ($cDNA_1$) and 5′-SH-ACA TTA CAG ATA GTA-3’ ($cDNA_2$) were obtained from Sangon Biotech Co., Ltd (Shanghai, China).

2.2. Preparation and amino-functionalization of PLNPs

ZGO:Mn was prepared via a hydrothermal method [37], and ZGGO:Cr was synthesized via a hydrothermal method combination with calcination [38]. The amino-functionalized PLNPs (NH_2-ZGO:Mn and NH_2-ZGGO:Cr) were obtained via the Stöber method using APTES as the silane coupling agent [39].

2.3. Surface modification of PLNPs with DNA

5 mg of NH_2-ZGO:Mn was dispersed in HEPES buffer (5 mL, 10 mM, pH 7.2) under sonication, then 1 mg of Sulfo-SMCC was added to the solution for 2 h reaction with shaking at 25 °C. The maleimide-activated NH_2-ZGO:Mn was obtained by centrifugation, rinsed with phosphate buffer saline (PBS) (10 mM, pH 7.4) three times, redispersed in 5 mL of PBS containing 5 nmol AFB_1 aptamer (Apt_1), and incubated at 25 °C overnight. Finally, the resulting AFB_1 aptamer modified ZGO:Mn (Apt_1-ZGO:Mn) were collected by centrifugation, washed with ultrapure water and redispersed in 5 mL of Tris-HCl buffer 1 (10 mM, pH 8.0, 100 mM NaCl) for further use. The ZEN aptamer modified ZGGO:Cr (Apt_2-ZGGO:Cr) was prepared in a similar way.

2.4. Surface modification of Fe_3O_4 with DNA

Amino-functionalized Fe_3O_4 (NH_2–Fe_3O_4) was prepared by a one-pot strategy [40]. Maleimide-activated NH_2–Fe_3O_4 was prepared in a similar procedure with Sulfo-SMCC as a bifunctional crosslinker as for the preparation of NH_2-ZGO:Mn. After magnetic separation, the activated NH_2–Fe_3O_4 was washed with PBS and then redispersed in PBS. To obtain $cDNA_1$ modified Fe_3O_4 ($cDNA_1$-Fe_3O_4), 3 nmol of $cDNA_1$ was mixed with the above maleimide-activated NH_2–Fe_3O_4 (3 mg) and shaking at 25 °C overnight. The resultant $cDNA_1$-Fe_3O_4 was separated by magnetic separation, washed with ultrapure water to remove excessive $cDNA_1$, and finally resuspended in 3 mL of Tris-HCl buffer 1 for further use. $cDNA_2$ modified Fe_3O_4 ($cDNA_2$-Fe_3O_4) was prepared using the similar procedure.

2.5. Fabrication of dual-colored PLNPs based nanosensor

Apt_1-ZGO:Mn was mixed with $cDNA_1$-Fe_3O_4 at a concentration ratio of 10:3 with gentle shaking for 50 min at 37 °C, the resultant Apt_1-ZGO:Mn@$cDNA_1$-Fe_3O_4 composites were separated by magnetic separation and washed with ultrapure water, and then resuspended in Tris-HCl buffer 2 (10 mM, pH 7.4, 100 mM NaCl). The Apt_2-ZGGO:Cr@$cDNA_2$-Fe_3O_4 composites were prepared in a similar way.

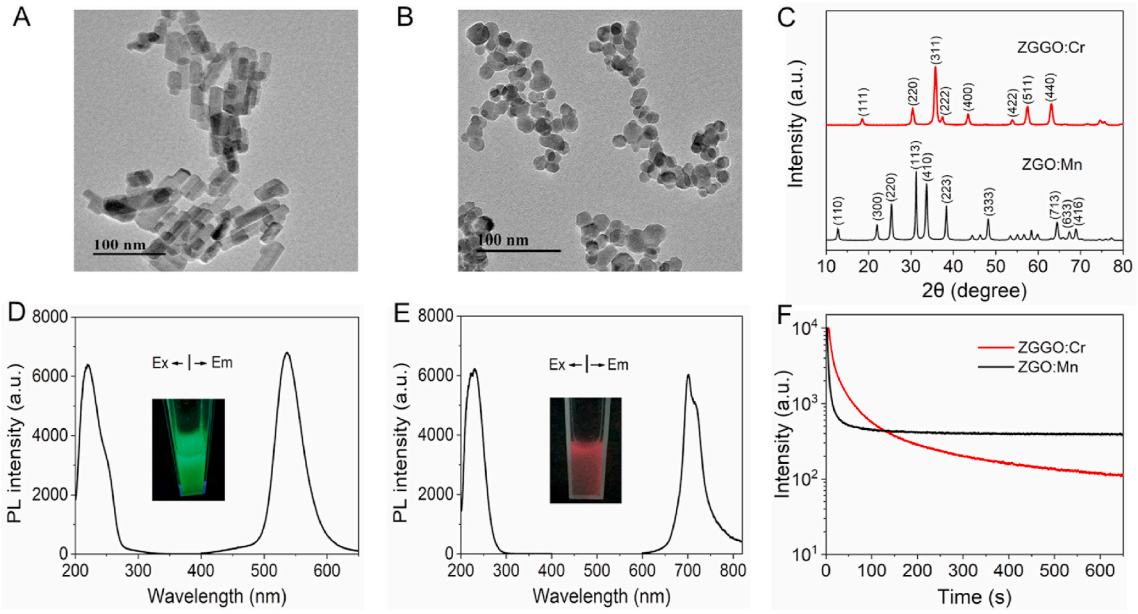

Fig. 1. TEM images: (A) ZGO:Mn; (B) ZGGO:Cr. (C) XRD patterns of ZGO:Mn and ZGGO:Cr. Excitation and emission spectra: (D) ZGO:Mn; (E) ZGGO:Cr. Inset: photograph of the PLNPs solution under 254 nm UV excitation. (F) Persistent luminescence decay curves of ZGO:Mn and ZGGO:Cr.

2.6. Sample preparation

Grain samples were collected from a local market and extracted according to an official method [41,42]. Briefly, 5.0 g of the fine ground sample and 0.5 g NaCl were mixed with 20 mL of 84% acetonitrile aqueous solution under ultrasonication for 20 min, then the solution was centrifuged at 6000 rpm for 10 min. The obtained supernatant was filtered through a 0.22 μm membrane filter and then diluted to 100 mL with ultrapure water. For the recovery study, the grain samples were spiked with various amounts of AFB_1 and ZEN standard solutions before extraction.

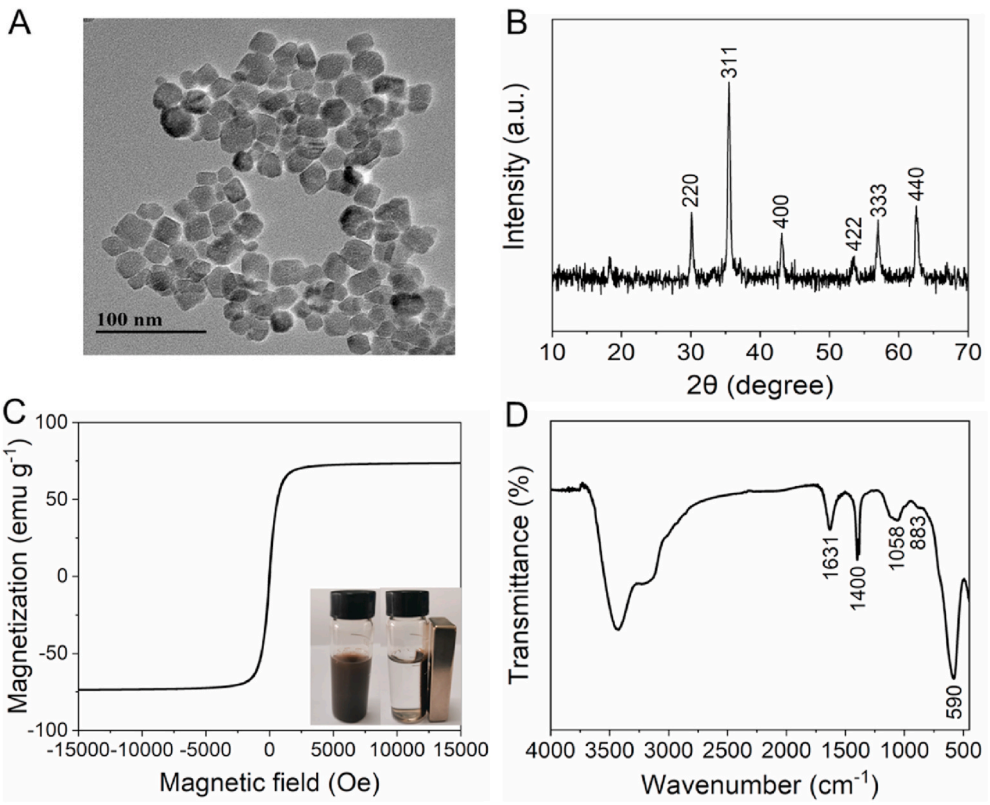

Fig. 2. Characterization of the as-prepared NH_2–Fe_3O_4: (A) TEM image; (B) XRD pattern; (C) Magnetization curves; (D) FT-IR spectrum. The inset shows the photograph of the water dispersion of NH_2–Fe_3O_4 before and after exposure to an external magnetic field.

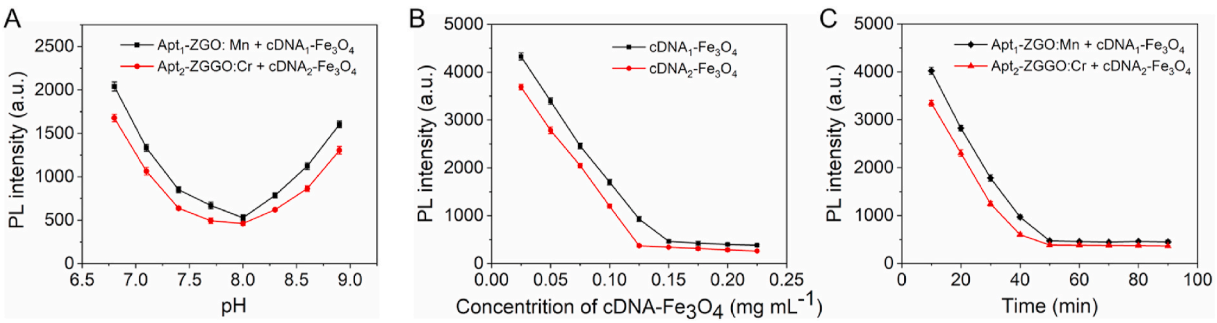

Fig. 3. Optimization of the fabrication of Apt-PLNPs@cDNA-Fe_3O_4 (Apt-PLNPs, 0.5 mg mL^{-1}): (A) pH; (B) cDNA-Fe_3O_4 concentration; (C) hybridization time.

2.7. Procedures for the determination of AFB_1 and ZEN

150 μL of Apt_1-ZGO:Mn@$cDNA_1$-Fe_3O_4 (1 mg mL^{-1}) and 150 μL of Apt_2-ZGGO:Cr@ $cDNA_2$-Fe_3O_4 (1 mg mL^{-1}) were mixed, and then 40 μL of the standard solution of AFB_1 and ZEN or sample solution were added. The mixture solution was made to 400 μL with Tris-HCl buffer 2 for 40 min incubation at 37 °C, the unreactive Apt-PLNPs@cDNA-Fe_3O_4 and the replaced cDNA-Fe_3O_4 were then separated by magnetic separation and washed with Tris-HCl buffer 2, while all of the supernatant containing Apt-PLNPs signal units were collected and made to 1 mL with Tris-HCl buffer 2. The persistent luminescence (PL) was recorded on an F-7000 spectrometer (Hitachi, Japan) in the phosphorescence mode with excitation wavelength of 254 nm.

3. Results and discussion

3.1. Design and characterization of dual-colored PLNPs based nanosensor

Scheme 1 illustrates the basic principle of the dual-colored PLNPs labeling and magnetic separation based nanosensor for the simultaneous determination of AFB_1 and ZEN. Briefly, AFB_1 aptamer modified ZGO:Mn (Apt_1-ZGO:Mn) and its partially complementary DNA modified Fe_3O_4 ($cDNA_1$-Fe_3O_4) are assembled through the hybridization of Apt_1 with $cDNA_1$, then the formed Apt_1-ZGO:Mn@$cDNA_1$-Fe_3O_4 are obtained by magnetic separation. The persistent luminescence intensity of Apt_1-ZGO:Mn in supernatant at 537 nm is at a minimum in the absence of AFB_1, but increases in the presence of AFB_1 due to the release of the Apt_1-ZGO:Mn from Apt_1-ZGO:Mn@$cDNA_1$-Fe_3O_4 due to the high affinity between the Apt_1 and AFB_1. Similarly, the presence of ZEN enables the release of the Apt_2-ZGGO:Cr from Apt_2-ZGGO:Cr@$cDNA_2$-Fe_3O_4 due to the high affinity between Apt_2 and ZEN, and enhances the persistent luminescence intensity of ZGGO:Cr-Apt_2-ZEN in supernatant at 701 nm. Therefore, multiple mycotoxins AFB_1 and ZEN can be detected simultaneously by monitoring the change of dual distinguishable luminescence signals at 537 and 701 nm with a single excitation.

The prepared ZGO:Mn was monodispersed nanorods with the size of 48 ± 5 nm × 12 ± 1 nm (Fig. 1A) as well as a standard rhombohedral phase of zinc germanate (Fig. 1C), and gave a bright green luminescence emission at 537 nm originating from the $^4T_1$ (4G)-$^6A_1$ (^6S) transition of Mn^{2+} ions with an excitation spectrum from 200 nm to 270 nm (Fig. 1D). The prepared ZGGO:Cr were spherical nanoparticle with the size of 20 ± 1 nm (Fig. 1B) and a pure spinel phase structure of zinc gallogermanate (Fig. 1C). ZGGO:Cr emitted near infrared luminescence at 701 nm due to the $^2E \rightarrow {}^4A_2$ transition of distorted Cr^{3+} ions with an excitation spectrum from 200 nm to 280 nm. Both ZGO:Mn and ZGGO:Cr exhibited excellent long-lasting persistent luminescence after a UV lamp irradiation for 5 min (Fig. 1F). Additionally, ZGO:Mn and ZGGO:Cr gave stable luminescence over 12 h at a certain pH in a pH range of 6.5–9.5 (Fig. S1).

The prepared PLNPs were first modified with amino group and then conjugated with cDNA. The N–H stretching bands at 3416 and 3245 cm^{-1}, asymmetric and symmetric stretching bands of –CH_2– at 2930 and 2875 cm^{-1} and the strong stretching vibrations of O–Si–O at 1121 and 1035 cm^{-1} indicate the successful amino functionalization of PLNPs (Fig. S3). The zeta potential of NH_2-ZGO:Mn and NH_2-ZGGO:Cr in Tris-HCl buffer (pH 8.0) was 19.4 and 17.1 mV, respectively, but became −29.8 and −26.5 mV, respectively, after further modification with the aptamers (Fig. S4), indicating the successful conjugation of PLNPs with aptamers.

The prepared NH_2–Fe_3O_4 displayed good dispersibility with an average size of 25 ± 3 nm (Fig. 2A), a pure magnetite phase (Fig. 2B), and a saturation magnetization value of 73.1 emu g^{-1} (Fig. 2C). The vibration band at 590 cm^{-1} for Fe–O and the characteristic bands at 1631, 1400, 1058 and 883 cm^{-1} for amino groups indicate the existence of –NH_2 on the surface of Fe_3O_4 (Fig. 2D). cDNA functionalization made the zeta potential of NH_2–Fe_3O_4 in Tris-HCl buffer (pH 8.0) change from −9.3 mV to −25.3 and −23.6 mV for $cDNA_1$-Fe_3O_4 and $cDNA_2$-Fe_3O_4, respectively, due to the phosphoric acid skeleton of the aptamer

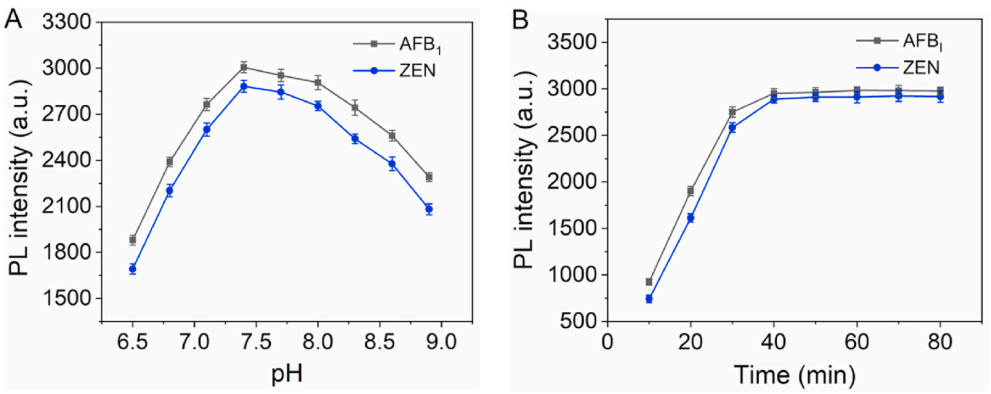

Fig. 4. Effect of pH (A) and reaction time (B) on the PL intensity responses of the nanosensor in the presence of 10 ng mL^{-1} of AFB_1 and ZEN.

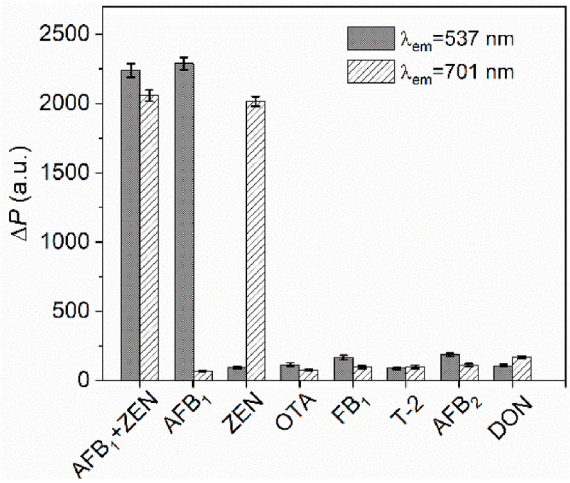

Fig. 5. Cross reactivity and selectivity of the nanosensor in the presence of different toxins (AFB_1 and ZEN: 1 ng mL^{-1}, all other toxins: 10 ng mL^{-1}).

(Fig. S4). Besides, cDNA-Fe_3O_4 possessed bigger hydrodynamic size than NH_2–Fe_3O_4 (Fig. S5).

3.2. Optimization of the developed nanosensor

Important factors including pH, cDNA-Fe_3O_4 concentration and reaction time which might affect the hybridization between Apt-PLNPs and cDNA-Fe_3O_4 were optimized first. Study on the effect of pH showed that pH 8.0 was best for the DNA hybridization (Fig. 3A). The effect of cDNA-Fe_3O_4 concentration was studied with 0.5 mg mL^{-1} of Apt-PLNPs at pH 8.0. The luminescence intensity of Apt-PLNPs in supernatant after magnetic separation diminished gradually with the increase of cDNA-Fe_3O_4 concentration owing to the conjugation of Apt-PLNPs with cDNA-Fe_3O_4 (Fig. 3B), then reached a plateau over 0.15 mg mL^{-1} $cDNA_1$-Fe_3O_4 and 0.125 mg mL^{-1} $cDNA_2$-Fe_3O_4, respectively. Additionally, the luminescence intensity of supernatant decreased rapidly in the first 40 min, and then leveled off with further increase of hybridization time (Fig. 3C). Therefore, 50 min was chosen as the hybridization time.

We then examined the effects of pH and reaction time on the release of the Apt-PLNPs from 0.5 mg mL^{-1} Apt-PLNPs@cDNA-Fe_3O_4 by 10 ng mL^{-1} AFB_1 and ZEN. The luminescence of the signal units in supernatant increased as pH increased to 7.4, then decreased as pH further increased (Fig. 4A). The result indicates that the optimal pH for the binding of the aptamer to target was 7.4. Study on the effect of reaction time showed that the luminescence of the signal units in supernatant exhibited a rapid increase in the first 40 min and then levelled off (Fig. 4B), showing the binding of aptamer to target was complete in 40 min.

3.3. Cross reaction and specificity of the nanosensor

The luminescence recovery by AFB_1 and ZEN (all at 1 ng mL^{-1}) was measured to rate the cross reaction of the nanosensor. Fig. 5 shows that the luminescence signals at 537 nm and 701 nm simultaneously enhanced when AFB_1 and ZEN coexisted. In contrast, the luminescence increased at 537 nm only in the presence of AFB_1, and at 701 nm only in the presence of ZEN. The above results indicate no cross reactivity during simultaneous detection of AFB_1 and ZEN.

Five other toxins including ochratoxin A (OTA), fumonisin B_1 (FB_1), trichothecenes A (T-2), aflatoxin B_2 (AFB_2), and deoxynivalenol (DON) (all at 10 ng mL^{-1}) to assess the specificity of the proposed nanosensor for the determination of AFB_1 and ZEN at 1 ng mL^{-1}. Fig. 5 shows that only AFB_1 and ZEN induced remarked persistent luminescence, while no other toxins studied produced significant luminescence change even at a ten times concentration. These results demonstrate that the developed nanosensor possesses high specificity to AFB_1 and ZEN.

3.4. Figures of merit of the developed nanosensor

Under optimal conditions, the luminescence intensity increased with the concentration of AFB_1 and ZEN (Fig. 6A), and the increased luminescence intensity (ΔP) increased linearly with the logarithm of the concentration of AFB_1 and ZEN (C_{AFB1} and C_{ZEN}, ng mL^{-1}) in a wide range from 0.001 ng mL^{-1} to 50 ng mL^{-1} (Fig. 6B). The calibration functions for the determination of AFB_1 and ZEN were $\Delta P = 602.1 \lg C_{AFB1} + 2194.6$ ($R^2 = 0.9985$) and $\Delta P = 663.2 \lg C_{ZEN} + 2090.6$ ($R^2 = 0.9972$), respectively. The limits of detection (LODs) (3s) were 0.29 and 0.22 pg mL^{-1}, respectively. Comparison with some reported methods for simultaneous detection of AFB_1 and ZEN shows that the proposed assay displayed comparable or even much lower LODs with wider linear range (Table S1). The relative standard deviations for 11 replicate determinations of AFB_1 and ZEN at 1 ng mL^{-1} were 2.1% and 2.3%, respectively.

3.5. Validation and application of the developed nanosensor

The developed method was validated by analyzing a certified reference material (MRM0753) for AFB_1 and ZEN in corn. The concentrations of AFB_1 and ZEN determined in MRM0753 by the developed nanosensor were 27.4 ± 1.6 μg kg^{-1} ($n = 5$) and 71.3 ± 4.0 μg kg^{-1} ($n = 5$), in good agreement with the certified values of 26.5 ± 5.3 μg kg^{-1} and 74 ± 15 μg kg^{-1}, respectively, demonstrating the high accuracy of the developed nanosensor. The developed nanosensor was also applied to the

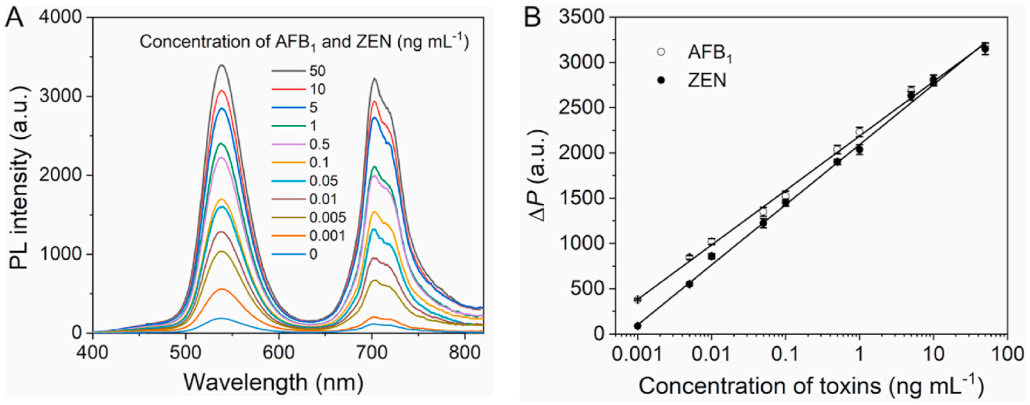

Fig. 6. (A) PL signals of the nanosensor at different concentrations of AFB_1 and ZEN. (B) Plot of the increased PL intensity (ΔP) against the concentration of AFB_1 or ZEN.

Table 1
Analytical results for the determination of AFB_1 and ZEN in grain samples.

Samples		Concentration determined ($\mu g\ kg^{-1}$, mean ± s, $n = 3$)	Recovery for 0.5 $\mu g\ kg^{-1}$ spiked AFB_1 and ZEN (%) (mean ± s, $n = 3$)
Corn	AFB_1	ND (not detected)	96.5 ± 3.7
	ZEN	0.726 ± 0.035	101.2 ± 5.6
Rice	AFB_1	ND	95.8 ± 4.9
	ZEN	ND	94.7 ± 3.2
Oats	AFB_1	0.287 ± 0.013	96.6 ± 7.1
	ZEN	ND	95.9 ± 2.6
Wheat	AFB_1	ND	93.6 ± 4.2
	ZEN	1.335 ± 0.072	97.3 ± 6.7
Millet	AFB_1	ND	103.2 ± 5.0
	ZEN	ND	98.4 ± 2.8
Corn grit	AFB_1	0.406 ± 0.021	97.1 ± 6.6
	ZEN	0.971 ± 0.054	105.1 ± 4.9

determination of AFB_1 and ZEN in various grain samples to demonstrate its applicability in real sample analysis. The analytical results are summarized in Table 1. The recoveries for spiked AFB_1 and ZEN were in the range of 93.6%–103.2% and 94.7%–105.1%, respectively. The above results demonstrate the practical feasibility of the developed nanosensor for the simultaneous determination of AFB_1 and ZEN in real samples.

4. Conclusions

In summary, we have developed a nanosensor using dual-colored PLNPs labeling and magnetic separation for simultaneous determination of AFB_1 and ZEN in food samples. The proposed nanosensor combines the merits of autofluorescence-free detection of persistent luminescence, the high specificity of aptamer and the high speed of magnetic separation, allows highly sensitive and selective detection of AFB_1 and ZEN in complex samples. In addition, the developed method can also be extendable to other analytes just by replacing the aptamer and cDNA, providing a universal optical platform for simultaneous determination of multi contaminants in complex samples.

Credit author statement

Yuan-Yuan Jiang: Conceptualization, Investigation, Methodology, Data curation, Writing - original draft. **Xu Zhao:** Methodology, Investigation. **Li-Jian Chen:** Methodology, Validation. **Cheng Yang:** Validation. **Xue-Bo Yin:** Supervision. **Xiu-Ping Yan:** Conceptualization, Supervision, Writing - review & editing, Funding acquisition.

Declaration of competing interest

We declare no competing financial interest.

Acknowledgments

The authors appreciate the financial supports from the National Natural Science Foundation of China (No. 21934002, 21804056 and 21804057), the National First-class Discipline Program of Food Science and Technology (No. JUFSTR20180301), and the Program of "Collaborative Innovation Center of Food Safety and Quality Control in Jiangsu Province".

Appendix A. Supplementary data

Supplementary data to this article can be found online at https://doi.org/10.1016/j.talanta.2021.122395.

References

[1] S. Marin, A.J. Ramos, G. Cano-Sancho, V. Sanchis, Mycotoxins: occurrence, toxicology, and exposure assessment, Food Chem. Toxicol. 60 (2010) 218–237.
[2] H.S. Hussein, J.M. Brasel, Toxicity, metabolism, and impact of mycotoxins on humans and animals, Toxicology 167 (2001) 101–134.
[3] J.W. Bennett, M. Klich, Mycotoxins, Clin. Microbiol. Rev. 16 (2003) 497–516.
[4] Z. Liu, Q. Hua, J. Wang, Z. Liang, J. Li, J. Wu, X. Shen, H. Lei, X. Li, A smartphone-based dual detection mode device integrated with two lateral flow immunoassays for multiplex mycotoxins in cereals, Biosens. Bioelectron 158 (2020) 112178.
[5] X. Ding, P. Li, Y. Bai, H. Zhou, Aflatoxin B_1 in post-harvest peanuts and dietary risk in China, Food Contr. 23 (2012) 143–148.
[6] P.D. Andrade, R.R. Dantas, T.L.d.S.d. Moura-Alves, E.D. Caldas, Determination of multi-mycotoxins in cereals and of total fumonisins in maize products using isotope labeled internal standard and liquid chromatography/tandem mass spectrometry with positive ionization, J. Chromatogr. A 1490 (2017) 138–147.
[7] A.B. Serrano, G. Font, M.J. Ruiz, E. Ferrer, Co-occurrence and risk assessment of mycotoxins in food and diet from mediterranean area, Food Chem. 135 (2012) 423–429.
[8] C. Yang, G. Song, W. Lim, Effects of mycotoxin-contaminated feed on farm animals, J. Hazard Mater. 389 (2020) 122087.
[9] S.K. Pankaj, H. Shi, K.M. Keener, A review of novel physical and chemical decontamination technologies for aflatoxin in food, Trends Food Sci. Technol. 71 (2018) 73–83.
[10] R. Liu, W. Li, T. Cai, Y. Deng, Z. Ding, Y. Liu, X. Zhu, X. Wang, J. Liu, B. Liang, T. Zheng, J. Li, TiO_2 nanolayer-enhanced fluorescence for simultaneous multiplex mycotoxin detection by aptamer microarrays on a porous silicon surface, ACS Appl. Mater. Interfaces 10 (2018) 14447–14453.
[11] J. Qian, C. Ren, C. Wang, W. Chen, X. Lu, H. Li, Q. Liu, N. Hao, H. Li, K. Wang, Magnetically controlled fluorescence aptasensor for simultaneous determination of ochratoxin A and aflatoxin B1, Anal. Chim. Acta 1019 (2018) 119–127.
[12] I.M. Khan, S. Niazi, Y. Yu, A. Mohsin, B.S. Mushtaq, M.W. Iqbal, A. Rehman, W. Akhtar, Z. Wang, Aptamer induced multicolored AuNCs-WS_2 "turn on" FRET nano platform for dual-color simultaneous detection of aflatoxin B_1 and zearalenone, Anal. Chem. 91 (2019) 14085–14092.
[13] Y. Liu, W. Li, Z. Ding, Q. Li, X. Wang, J. Liu, S. Zhuo, R. Shao, Q. Ling, T. Zheng, J. Li, Three-dimensional ordered macroporous magnetic photonic crystal microspheres for enrichment and detection of mycotoxins (II): the application in liquid chromatography with fluorescence detector for mycotoxins, J. Chromatogr. A 1604 (2019) 460475.
[14] A.K. Rausch, R. Brockmeyer, T. Schwerdtle, Development and validation of a QuEChERS-based liquid chromatography tandem mass spectrometry multi-method for the determination of 38 native and modified mycotoxins in cereals, J. Agric. Food Chem. 68 (2020) 4657–4669.
[15] E. Van Pamel, A. Verbeken, G. Vlaemynck, J. De Boever, E. Daeseleire, Ultrahigh-performance liquid chromatographic-tandem mass spectrometric multimycotoxin method for quantitating 26 mycotoxins in maize silage, J. Agric. Food Chem. 59 (2011) 9747–9755.
[16] Y. Shao, H. Duan, S. Zhou, T. Ma, L. Guo, X. Huang, Y. Xiong, Biotin-streptavidin system-mediated ratiometric multiplex immunochromatographic assay for simultaneous and accurate quantification of three mycotoxins, J. Agric. Food Chem. 67 (2019) 9022–9031.
[17] S. Hou, J. Ma, Y. Cheng, H. Wang, J. Sun, Y. Yan, Quantum dot nanobead-based fluorescent immunochromatographic assay for simultaneous quantitative detection of fumonisin B_1, dexyonivalenol, and zearalenone in grains, Food Contr. 117 (2020) 107331.
[18] L. Lu, R.S. Seenivasan, Y.C. Wang, J.H. Yu, S. Gunasekaran, An electrochemical immunosensor for rapid and sensitive detection of mycotoxins fumonisin B1 and deoxynivalenol, Electrochim. Acta 213 (2016) 89–97.
[19] Z. Han, Z. Tang, K. Jiang, Q. Huang, J. Meng, D. Nie, Z. Zhao, Dual-target electrochemical aptasensor based on co-reduced molybdenum disulfide and Au NPs (rMoS_2-Au) for multiplex detection of mycotoxins, Biosens. Bioelectron. 150 (2020) 111894.
[20] Z. Pan, Y.Y. Lu, F. Liu, Sunlight-activated long-persistent luminescence in the near-infrared from Cr^{3+}-doped zinc gallogermanates, Nat. Mater. 11 (2012) 58–63.
[21] Y. Li, M. Gecevicius, J. Qiu, Long persistent phosphors-from fundamentals to applications, Chem. Soc. Rev. 45 (2016) 2090–2136.
[22] J. Wang, Q. Ma, Y. Wang, H. Shen, Q. Yuan, Recent progress in biomedical applications of persistent luminescence nanoparticles, Nanoscale 9 (2017) 6204.
[23] S.K. Sun, H.F. Wang, X.P. Yan, Engineering persistent luminescence nanoparticles for biological applications: from biosensing/bioimaging to theranostics, Acc. Chem. Res. 51 (2018) 1131–1143.
[24] B.Y. Wu, H.F. Wang, J.T. Chen, X.P. Yan, Fluorescence resonance energy transfer inhibition assay for α-fetoprotein excreted during cancer cell growth using functionalized persistent luminescence nanoparticles, J. Am. Chem. Soc. 133 (2011) 686–688.
[25] B.Y. Wu, X.P. Yan, Bioconjugated persistent luminescence nanoparticles for föster resonance energy transfer immunoassay of prostate specific antigen in serum and cell extracts without in situ excitation, Chem. Commun. 51 (2015) 3903–3906.
[26] F. Feng, X. Chen, G. Li, S. Liang, Z. Hong, H.F. Wang, Afterglow resonance energy transfer inhibition for fibroblast activation protein-α assay, ACS Sens. 3 (2018) 1846–1854.
[27] Y. Wang, Z. Li, Q. Lin, Y. Wei, J. Wang, Y. Li, R. Yang, Q. Yuan, Highly sensitive detection of bladder cancer-related miRNA in urine using time-gated luminescent biochip, ACS Sens. 4 (2019) 2124–2130.

[28] L. Shi, J. Shao, X. Jing, W. Zheng, H. Liu, Y. Zhao, Autoluminescence-free dual tumor marker biosensing by persistent luminescence nanostructures, ACS Sustain. Chem. Eng. 8 (2020) 686–694.
[29] Y.Y. Jiang, X. Zhao, L.J. Chen, C. Yang, X.B. Yin, X.P. Yan, Persistent luminescence nanorod based luminescence resonance energy transfer aptasensor for autofluorescence-free detection of mycotoxin, Talanta 218 (2020) 121101.
[30] k. Ge, J. Liu, P. Wang, G. Fang, D. Zhang, S. Wang, Near-infrared-emitting persistent luminescent nanoparticles modified with gold nanorods as multifunctional probes for detection of arsenic (III), Microchim. Acta 186 (2019) 197.
[31] Y. Feng, D. Deng, L. Zhang, R. Liu, Y. L, LRET-based functional persistent luminescence nanoprobe for imaging and detection of cyanide ion, Sensor. Actuator. B Chem. 279 (2019) 189–196.
[32] R.H. Wang, C.L. Zhu, L.L. Wang, L.Z. Xu, W.L. Wang, C. Yang, Y. Zhang, Dual-modal aptasensor for the detection of isocarbophos in vegetables, Talanta 205 (2019) 120094.
[33] N. Li, Y. Li, Y. Han, W. Pan, T. Zhang, B. Tang, A highly selective and instantaneous nanoprobe for detection and imaging of ascorbic acid in living cells and in vivo, Anal. Chem. 86 (2014) 3924–3930.
[34] Y. Feng, H. Song, D. Deng, Y. L, Engineering ratiometric persistent luminous sensor arrays for biothiols identification, Anal. Chem. 92 (2020) 6645–6653.
[35] L.C. Le, J.A. Cruz-Aguado, G.A. Penner, DNA Ligands for Aflatoxin and Zearalenone. Patent: PCT/CA2010/001292, NeoVentures Biotechnology Inc., 2011.
[36] X. Chen, Y. Huang, N. Duan, S. Wu, X. Ma, Y. Xia, C. Zhu, Y. Jiang, Z. Wang, Selection and identification of ssDNA aptamers recognizing zearalenone, Anal. Bioanal. Chem. 405 (2013) 6573–6581.
[37] J. Wang, Q. Ma, W. Zheng, H. Liu, C. Yin, F. Wang, X. Chen, Q. Yuan, W. Tan, One-dimensional luminous nanorods featuring tunable persistent luminescence for autofluorescence-free biosensing, ACS Nano 11 (2017) 8185–8191.
[38] Y.J. Li, X.P. Yan, Synthesis of functionalized triple-doped zinc gallogermanate nanoparticles with superlong near-infrared persistent luminescence for long-term orally administrated bioimaging, Nanoscale 8 (2016) 14965–14970.
[39] A. Abdukayum, J.T. Chen, Q. Zhao, X.P. Yan, Functional near infrared-emitting Cr^{3+}/Pr^{3+} co-doped zinc gallogermanate persistent luminescent nanoparticles with superlong afterglow for in vivo targeted bioimaging, J. Am. Chem. Soc. 135 (2013) 14125–14133.
[40] L. Wang, J. Bao, L. Wang, F. Zhang, Y. Li, One-pot synthesis and bioapplication of amine-functionalized magnetite nanoparticles and hollow nanospheres, Chem. Eur J. 12 (2006) 6341–6347.
[41] GB 5009.22-2016, National Food Safety Standard for the Determination of Aflatoxin B and G in Foods, 5009, National Standards of the People's Republic of China, 2016.
[42] GB 5009.209-2016, National Food Safety Standard for the Determination of Zearalenone in Foods, 5009, National Standards of the People's Republic of China, 2016.